Sun et al. *NPG Asia Materials* (2022) 14:86
https://doi.org/10.1038/s41427-022-00434-z

NPG Asia Materials

ARTICLE Open Access

Mussel-inspired hydrogel with injectable self-healing and antibacterial properties promotes wound healing in burn wound infection

Ao Sun[1], Danrong Hu[1], Xinye He[1], Xiao Ji[1], Tao Li[2], Xiawei Wei[1,3] and Zhiyong Qian[1]

Abstract

Burn wound infections cause serious problems for public health. More than 180,000 patients die from burns every year worldwide. In addition, the difficulty of healing wounds and wound infections caused by burns affects the mental health of patients. Therefore, it is very important to develop a wound dressing that can promote wound repair and exhibits good antibacterial effects. Here, we used oxidized konjac glucomannan (OKGM), γ-poly(glutamic acid) modified with dopamine and L-cysteine (γ-PGA-DA-Cys) and ε-polylysine (ε-PL) to produce an OKGM/γ-PGA-DA-Cys/ε-PL (OKPP) hydrogel. This hydrogel was produced by thiol-aldehyde addition and Schiff-base reactions and has the ability to be injected and self-heal. The results showed that the hydrogel exhibits good antibacterial effects on *Pseudomonas aeruginosa* and *Staphylococcus aureus* and has antioxidant effects in vitro. Moreover, the hydrogel also exhibits good adhesion. In a burn wound infection model, the hydrogel promoted wound healing and reduced the production of inflammation. These results proved that the hydrogel has clinical potential as a wound dressing for burn wound infection.

Introduction

According to the WHO, more than 11 million people need treatments for burns every year, and more than 180,000 people die from burns. Burn infections are the main cause of these serious consequences[1,2]. Skin is an important barrier for the human body to resist harmful external pathogens. Burning destroys the integrity of skin, resulting in microbial invasion and infection[3]. At the same time, a large amount of necrotic tissue and protein-rich exudate in burn wounds are conducive to the reproduction and invasion of pathogenic microorganisms. It leads to the aggravation of wound infection, which will further lead to serious complications such as sepsis and ultimately endanger life[4,5]. Therefore, burn wound infections place a serious burden on the health of patients.

The main methods for treating burn wound infection are systemic antibiotic treatment, skin transplantation and wound dressing[6–8]. However, the frequent use of antibiotics leads to alterations in infectious flora and the risk of drug-resistant bacteria. There is a limited supply of skin for autologous skin transplantation, and allogeneic skin transplantation may lead to rejection. All methods must prevent the risk of infection to avoid chronic inflammation and delayed healing due to infection[9–11]. Most of the biological dressings currently used in burn treatments are made of hydrogels. Compared to traditional wound dressings, which stimulate the skin, are dry and lack effective protection, hydrogels have a unique three-dimensional network and high hydrophilicity, providing a moist healing environment, biocompatibility, and degradability[12,13]. At present, biological wound dressings are usually composed of natural polymers, such as chitosan and sodium alginate,

Correspondence: Xiawei Wei (xiaweiwei@scu.edu.cn) or Zhiyong Qian (anderson-qian@163.com)
[1]State Key Laboratory of Biotherapy/Collaborative Innovation Center for Biotherapy, West China Hospital, West China Medical School, Sichuan University, 610041 Chengdu, P.R. China
[2]Department of Cardiovascular Surgery, West China Hospital, Sichuan University, 610041 Chengdu, P.R. China
Full list of author information is available at the end of the article

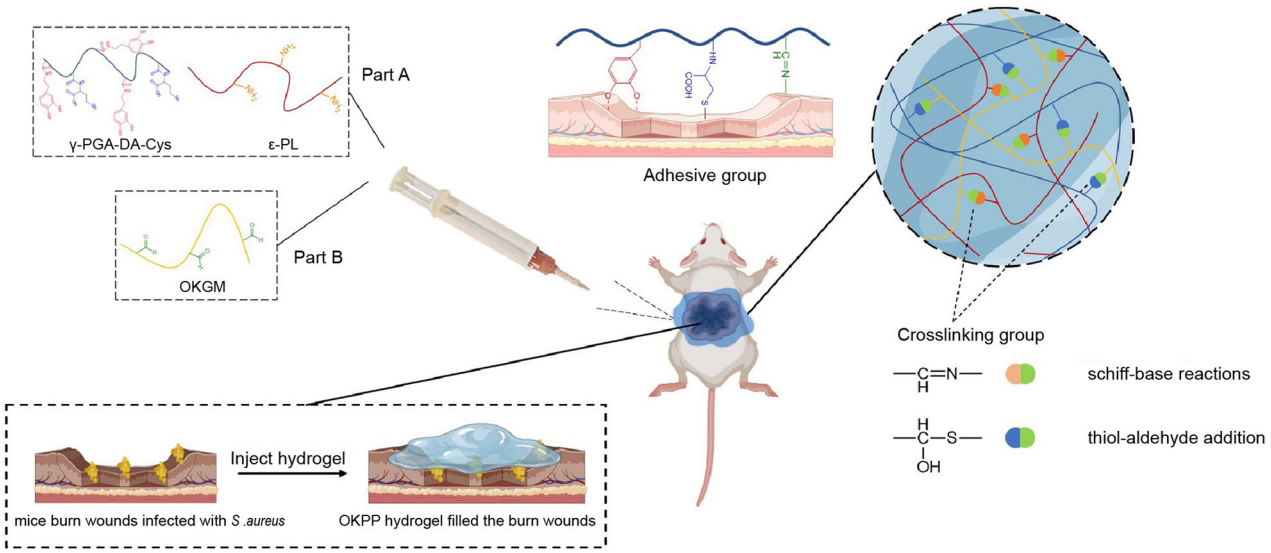

Fig. 1 Schematic representation of OKPP hydrogel synthesis and treatment of burn wound infection. The schematic showed the composition of OKPP hydrogel and the origin of adhesion properties. The OKPP hydrogel was introduced into the wound with a double-barrel syringe gun.

as well as antibacterial components, such as silver ions and antibacterial peptides[14–18]. The dressings have a local antibacterial effect and reduce the risk of antibiotic resistance. However, some studies have proven that severe inflammatory reactions and excessive oxidative stress caused by burn infection (such as excessive ROS production leading to tissue damage) may slow wound healing[4,19]. Biological wound dressings involve the risk of rupture; in addition, the wound may be irregular and difficult to fit[20,21]. On this basis, we need to build an injectable wound dressing that reduces inflammation, performs self-healing and can be fit long-term.

Konjac glucomannan (KGM), a water-soluble polysaccharide, is composed of d-mannose, d-glucose, and acetyl groups irregularly connected to glycosyl units. KGM has good biocompatibility and can also stimulate the proliferation of fibroblasts[22–26]. ε-polylysine (ε-PL), as a natural antibacterial polypeptide, is often added to food, has good biosafety, exhibits antibacterial activity against Gram-negative and Gram-positive bacteria, and makes it difficult for microorganisms to produce resistance[27–30]. γ-poly(glutamic acid) (γ-PGA) has good water solubility and biocompatibility, and the structure of γ-PGA is similar to that of ECM. γ-PGA can provide a good living environment and repair environment for cells. In addition, γ-PGA-containing hydrogels exhibit good mechanical properties and have enough mechanical strength to adapt to changes in the external environment as a skin barrier substitute to resist the infection of external microorganisms[31–35]. Therefore, the KGM, γ-PGA and ε-PL used to construct wound dressings have good application potential in the treatment of burn-infected skin. In addition, L-cysteine exhibits good antioxidant activity[36–38]. Modifying the γ-PGA chain can endow γ-PGA with certain antioxidant activity, which can reduce reactive oxygen species (ROS) at the wound and reduce inflammation. The catechol group dopamine (DA) can be attached to various surfaces in a moist saline environment by hydrogen bonding and metal coordination[39–42]. DA can be modified on γ-PGA to enhance adhesion strength so that the wound dressing made of hydrogel can provide a long-term adhesive barrier for skin.

In this work, we prepared an OKGM/γ-PGA-DA-Cys/ε-PL (OKPP) hydrogel constructed from OKGM, ε-PL and γ-PGA modified by dopamine and L-cysteine. As shown in Fig. 1, the OKPP hydrogel has the ability to inject and self-heal through thiol-aldehyde addition and Schiff-base reactions, which can solve the problem of long-term use and gel breaking. The OKPP hydrogel has antioxidant properties and can scavenge free radicals. This hydrogel has good antibacterial effects on *Pseudomonas aeruginosa* and *Staphylococcus aureus* and exhibits strong adhesion. In the burn wound infection model, the OKPP hydrogel promoted wound healing and reduced the production of inflammatory factors. This hydrogel has good clinical potential as a wound dressing for burn wound infection.

Materials and methods

Materials

γ-PGA (Mn: 2000 kDa), ε-PL (Mn: 2–5 kDa), dopamine hydrochloride (DA) (purity ≥ 98%), L-cysteine hydrochloride (purity ≥ 98%), 1-ethyl-3-(3-dimethylaminopropyl)carbodiimide hydrochloride (EDC) (purity ≥ 98%), 2-(*N*-morpholino) ethanesulfonic acid (MES) (purity ≥

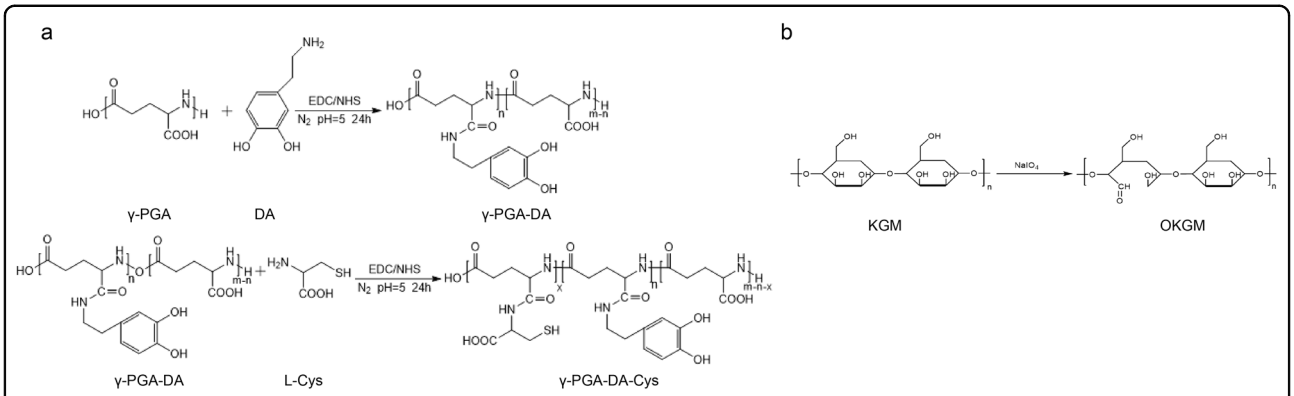

Fig. 2 Schematic representation of γ-PGA-DA-Cys and OKGM synthesis. **a** Synthesis of γ-PGA-DA and γ-PGA-DA-Cys. **b** Synthesis of OKGM.

99.5%), and *N*-hydroxysuccinimide (NHS) (purity ≥ 98%) were purchased from Aladdin Industrial Corporation. KGM (purity ≥ 98.0%) and sodium periodate (AR, purity ≥99.5%) were provided by Shanghai Macklin Biochemical Co., Ltd. (China).

Synthesis of γ-PGA-DA-Cys and OKGM

The synthesis method was described in the previous literature[43]. γ-PGA was dissolved in deionized (DI) water at a concentration of 5% (wt/vol) at 60 °C. After cooling to room temperature, EDC was added to the reaction solution and stirred for 30 min. Subsequently, dopamine hydrochloride and NHS were successively added to the mixture. The mixture was stirred under N_2 for 24 h, and the pH was subsequently adjusted to 5 (Fig. 2a). The reaction solution was dialyzed in 8–12 kDa dialysis bags for 72 h. The solution was lyophilized to obtain purified γ-PGA-DA.

γ-PGA-DA-Cys was prepared according to the literature procedures[34]. Briefly, γ-PGA-DA was dissolved in MES buffer (0.1 M MES, 0.1 M NaCl, pH 7.0), EDC was added to the reaction solution at room temperature and stirred for 30 min. Subsequently, L-cysteine hydrochloride dissolved in MES buffer and NHS were successively added to the mixture. The mixture was stirred under N_2 for 24 h, and the pH was subsequently adjusted to 5 (Fig. 2). The reaction solution was dialyzed in 8–12 kDa dialysis bags for 72 h. The solution was lyophilized to obtain purified γ-PGA-DA-Cys.

OKGM was prepared according to the literature procedures[25,44]. Briefly, KGM was dissolved in deionized (DI) water at a concentration of 1% (wt/vol) at 60 °C. At room temperature, 0.7 g sodium periodate was added to the reaction solution and stirred vigorously in the dark for 6 h (Fig. 2b). Then, ethylene glycol was added to the reaction mixture to react with excess periodate, and the mixture was stirred for another 2 h. The reaction solution was dialyzed in 8–12 kDa dialysis bags for 72 h. The reaction mixture was then centrifuged at 3000 rpm for 10 min. Finally, the supernatant was freeze-dried to obtain purified OKGM.

Preparation of the OKPP hydrogel

The OKPP hydrogel was cross-linked through the aldehyde group of OKGM and the thiol bond of γ-PGA-DA-Cys and the amino group of ε-PL to form a thiol-aldehyde addition and Schiff base. OKGM was dissolved in PBS (0.01 M, pH 7.4), and then γ-PGA-DA-Cys and ε-PL were dissolved in PBS (0.01 Next, the two solutions were mixed at room temperature for a certain time to obtain hydrogels. Four OKPP hydrogel systems were prepared by varying the ratios of the components.

Characterization

^{1}H-nuclear magnetic resonance (^{1}H-NMR) spectra of OKGM and γ-PGA-DA-Cys were measured using a 400 MHz ^{1}H-NMR (Bruker Inc., Germany), and D_2O was used as the solvent.

The Fourier transform infrared spectra (FT-IR) of OKGM and γ-PGA-DA-Cys were characterized by an ALPHA instrument (Bruker Daltonics, Bremen, Germany). The spectral range was 400–4000 cm^{-1}.

The dopamine content of γ-PGA-DA-Cys was determined by this method[40]. Briefly, nitrite molybdate reagent was added to the dopamine solution, and the reaction mixture was shaken. The pH of the solution was adjusted to 7.0 with NaOH aqueous solution, and the absorbance was measured at 520 nm with a UV-2600 spectrophotometer (Shimadzu).

The morphology of freeze-dried OKPP hydrogel was observed by scanning electron microscopy (SEM; JSM-7500 F; JEOL, Japan). The surface of the OKPP freeze-dried hydrogel was coated with gold prior to the observations.

The self-healing property of the OKPP hydrogel was verified by a macro self-healing experiment. The hydrogel plates were dyed and cut into two halves. Two alternately colored hydrogels were combined into a mixed whole

hydrogel disk and then placed at 25 °C for a few minutes. Subsequently, the healing hydrogel disk was lifted to check its self-healing ability.

The swelling ratio of the OKPP hydrogel was determined according to the literature method[44]. Each freeze-dried hydrogel had the same shape and size ($n = 3$). All freeze-dried hydrogels (weighted: W_0) were shaken for a period of time in PBS buffer at 37 °C. Then, the hydrogel was dried with filter paper (weighted: W_s).

The swelling ratio was calculated using the following equation: $SR = (W_S - W_0)/W_0 \times 100\%$.

Rheology test of the OKPP hydrogels

The rheological properties of the OKPP hydrogel were measured by a rotational HAAKE Rheostress 6000 rheometer (Thermo Scientific). The oscillatory rheology of the OKPP hydrogels was determined under linear viscoelastic conditions. The strain amplitude scanning was carried out in the range of 0.1–1000% at 1.0 Hz. At the same time, the critical strain region was studied by a strain amplitude scanning test. Next, the alternating strain scanning test was carried out at a fixed angular frequency (10 rad/s). The amplitude oscillation strain from low strain ($\gamma = 1.0\%$) switched to high strain ($\gamma = 300\%$), and each strain interval was 100 s. The shear thinning behavior of OKPP hydrogels (shear rate from 0.01 to 100 s^{-1}) was measured to measure the shear viscosity of hydrogels[21,45].

In vitro antibacterial properties of the OKPP hydrogels

According to the previous literature, the antibacterial activity of OKPP hydrogels was evaluated using *Pseudomonas aeruginosa* and *Staphylococcus aureus*[21,44]. Briefly, the bacteria were incubated in LB at 37 °C. The bacteria were then diluted with PBS to a concentration of 10^6 colony forming units (CFU)/mL. Two hundred microliters of OKPP hydrogel with different ratios was added to the wells of a 48-well microplate. Blank holes were used as the control group. Then, 100 μL of bacterial culture medium was inoculated onto the hydrogel surface of the 48-well plate and was incubated at 37 °C for 2 h. The bacteria in each well were diluted into different multiples with PBS, coated with LB agar plate, cultured at 37 °C for 24 h and counted colony forming units ($n = 3$). Experiments were carried out in triplicate for each preparation. Data were expressed as reduction as follows:

$$\mathrm{Log(reduction)} = \mathrm{log(cell\ count\ of\ control)} - \mathrm{log(cell\ count\ of\ control\ survivor\ count\ on\ hydrogels)}$$

Antioxidant efficiency of the OKPP hydrogels

The antioxidant properties of hydrogels were evaluated by the Gharibi method[46]. Briefly, the method was used to evaluate the efficiency of 1,1-diphenyl-2-picrylhydrazyl (DPPH) free radical scavenging by OKPP hydrogels. OKGM, γ-PGA-DA-Cys and OKPP hydrogel samples ($n = 3$) with different ratios (1 mg) of powder in liquid nitrogen. The dispersion of DPPH (3.0 mL, 0.1 M), and the sample (1 mg) in methanol was stirred and incubated in the dark for 15 min. Then, wavelength scanning was performed using a UV-2600 spectrophotometer (Shimadzu). DPPH degradation was calculated using the following equation:

$$\mathrm{DPPH\ scavenging}(\%) := \frac{\mathrm{Ab} - \mathrm{As}}{\mathrm{Ab}} \times 100\%$$

Ab is the absorption of the blank (DPPH + methanol), and As is the absorption of the sample (DPPH + methanol + sample).

Adhesive strength tests

The wet adhesive strength of hydrogels was evaluated by the lap shear strength test, which was carried out by a universal testing machine (Instron Model 4466, 50 N) according to the literature[28,40]. The tensile rate of the test at room temperature was set to 10 mm/min^{-1}. Briefly, 100 μL of hydrogel precursor solution was applied to two fresh pigskin surfaces (10 mm × 30 mm), and the adhesive area was also maintained at 10 mm × 10 mm after the gel was formed. The adherent pigskin was immediately put into the moist chamber (37 °C, 30 min). Subsequently, the adhesion strength of the hydrogel was tested. Each sample was at least fivefold, and the results were reported as averages.

Cytocompatibility evaluation of the hydrogel

The in vitro cytotoxicity of OKPP hydrogels was determined using MTT (3-(4,5-dimethyl-thiazol-2-yl)−2,5-diphenyl tetrazolium bromide) assays. The MTT test was used to quantitatively evaluate the cytotoxicity of the hydrogel on NIH 3T3 cells. Briefly, the OKPP hydrogels were immersed in Dulbecco's modified Eagle's medium containing 10% (v/v) fetal bovine serum for 8 h. Then, the hydrogel was removed, and the extract was obtained. NIH 3T3 cells at a concentration of 3×10^3 cells per well were added to 96-well culture plates and incubated overnight. Except for the control well, each well was treated with hydrogel extract. The cells were cultured for 24, 48, and 72 h. Cell viability was evaluated by MTT assay, and the OD (optical density) was measured at 490 nm by a microplate reader (iMark; Bio-Rad, Hercules, CA, USA).

Fluorescence microscopy was used to observe the live/dead NIH 3T3 cells that were retained after exposure to hydrogel. Briefly, NIH 3T3 cells were seeded in 48-well culture plates and incubated for 5 h, and then the hydrogel plates were placed in the wells. After culturing for 72 h, cell proliferation was detected by Calcein-AM/PI Double Staining Kits. The morphology of cells on the plate was

observed by fluorescence microscopy (SP 8, Leica). Control cells were implanted in pores without a hydrogel.

In vitro ROS scavenging effect of the OKPP hydrogel

The ROS scavenging ability of OKPP hydrogels in cells was studied based on previous literature[47]. Briefly, NIH 3T3 cells at a concentration of 3×10^3 cells per well were added to a 96-well culture plate and incubated overnight. Next, the hydrogel plates were placed in the well and incubated. After 30 min, the cells were treated with 250 μM H_2O_2 and incubated for 24 h. Cell viability was evaluated by MTT assay, and the OD was measured at 490 nm by a microplate reader (iMark; Bio-Rad, Hercules, CA, USA). Wells without H_2O_2 were negative controls.

In vivo wound healing

The burn-infection model was established in female BALB/c mice using reported methods[48]. Each mouse was anesthetized with isoflurane, and their back hair was shaved. The backs of the mice were burned with hot round copper (diameter 10 mm, 90 °C, 15 s) to induce deep partial thickness burns. After 1 day, the skin tissue at the burn site was cut off. A total of 100 μL of inoculum containing 10^8 CFU/mL *S. aureus* was applied evenly to the wound. After 12 h, the wound contained pus. Then, the wound was treated with 3 M Tegaderm™ commercial dressing or 200 μL OKPP hydrogel. In the OKPP hydrogel treatment, the mixed hydrogel precursor solution was introduced into the wound with a double-barrel syringe gun and then subjected to in situ gel electrophoresis. Untreated mice were used as a blank control ($n = 5$ for each group). The changes in mouse wounds were imaged with a digital camera on days 3, 7, 14, and 21. The exposed area of the wound was obtained using ImageJ software (NIH, Bethesda, MD, USA). Wound closure was calculated using the following formula: (area of original wound − area of actual wound)/area of original wound × 100%.

According to the literature, three groups of skin samples were collected on day 14[49]. The skin tissue around the wound was taken from each group and homogenized, diluted with PBS and then spread on LB plates ($n = 3$). The bacterial burden was evaluated at the wound in each group.

The mice were euthanized on days 4, 8, 12, and 16 after the operation. Skin tissue was fixed with 4% phosphate buffered paraformaldehyde and embedded in paraffin. The sections were stained with hematoxylin and eosin (H&E) and Masson's stain. Dyed stained sections were observed using an optical microscope (Leica, Wetzlar).

Immunohistochemical staining

To evaluate the inflammation and angiogenesis of wounds, immunohistochemistry was used to detect the expression of CD31 and TGF-β in wound tissue. The skin tissue was fixed with 4% phosphate buffered paraformaldehyde and embedded in paraffin. The sections were stained with CD31 and TGF-β immunostaining. Dyed stained sections were observed using an optical microscope (Leica, Wetzlar).

Results

Synthesis and characterization

The dopamine and L-cysteine modification of γ-PGA is carried out by amidation.^{1}H-NMR has demonstrated that dopamine and L-cysteine modify γ-PGA (Fig. 3a). Compared

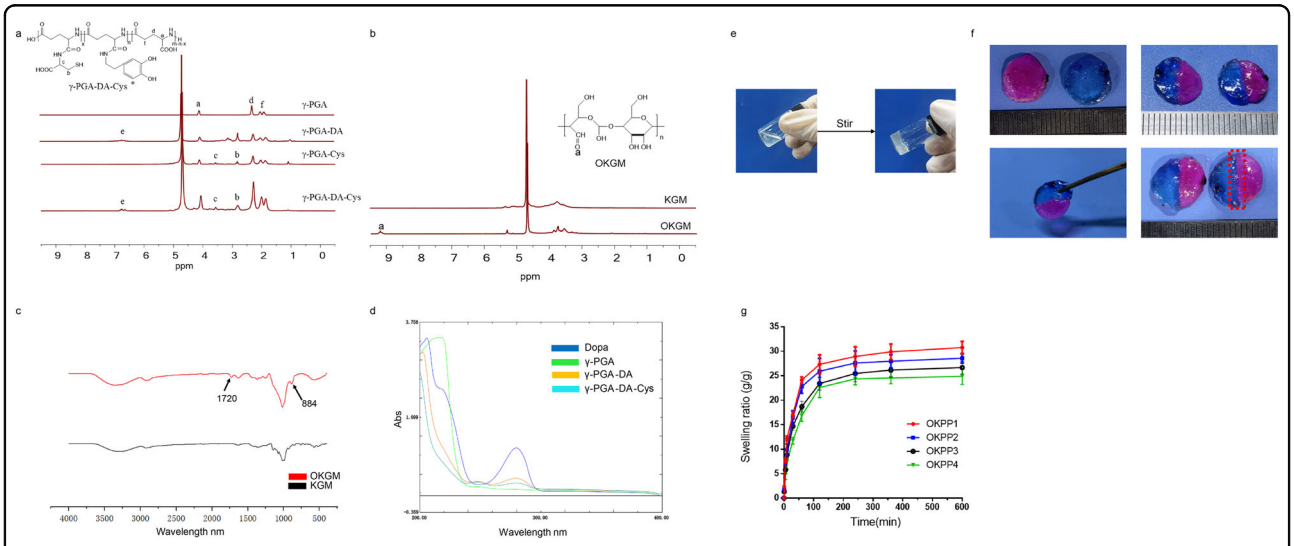

Fig. 3 Characterization of the OKPP hydrogels. a, **b** ^{1}H-NMR spectra of γ-PGA-DA-Cys and OKGM. **c** FT-IR spectrum of OKGM. **d** UV–vis spectra of different groups. **e**, **f** Self-healing ability of OKPP hydrogels. The boundary between hydrogels is blurred at the red dotted line. **g** Swelling ratio of OKPP hydrogels.

Table 1 The gelation times of the OKPP hydrogels with different concentrations.

Hydrogels	OKGM (wt%)	γ-PGA-DA-SH (wt %)	Gelation time (s)
OKPP 5 wt%	2.5	2.5	134 ± 10
OKPP 10 wt%	5	5	89 ± 12
OKPP 15 wt%	7.5	7.5	56 ± 6
OKPP 20 wt%	10	10	31 ± 2

Table 2 The components and gelation times of the OKPP hydrogels.

Hydrogels	OKGM (wt%)	γ-PGA-DA-SH (wt%)	ε-PL (wt %)	Gelation time (s)
OKPP1	7.5	7.5	0	56 ± 6
OKPP2	7.5	6.25	1.25	47 ± 5
OKPP3	7.5	5	2.5	38 ± 7
OKPP4	7.5	3.75	3.75	24 ± 3

with γ-PGA, γ-PGA-DA and γ-PGA-DA-Cys have additional signals at 6.8–7.0 ppm. This result indicated the successful conjugation of DA with the polymer backbone. In addition, we used a UV spectrophotometer to scan the wavelengths of γ-PGA-DA and γ-PGA-DA-Cys (Fig. 3d). They both have absorption peaks at 280 nm, confirming the successful introduction of DA moieties. The dopamine content of γ-PGA-DA-Cys was determined by Arnow's method to be 1.04 mmol/g, and the degree of substitution (DS) of dopamine was 15.38%. γ-PGA-Cys and γ-PGA-DA-Cys have additional signals at 2.8 ppm and 3.4 ppm, respectively. The signals belong to terminal methylene and methylene on L-cysteine, respectively[34,45]. This proved that L-cysteine was successfully modified on γ-PGA. Through ^{1}H-NMR, the DS of L-cysteine on γ-PGA-DA-Cys was determined to be 23.02%.

^{1}H-NMR showed that KGM was successfully oxidized to OKGM (Fig. 3b). Compared with KGM, OKGM has an additional signal at 9.2 ppm, corresponding to the aldehyde group in OKGM[44]. In addition, the FTIR spectrum of OKGM shows two characteristic bands at ~1720 cm^{-1} and 882 cm^{-1} (Fig. 3c). The band near 1720 cm^{-1} was attributed to carbonyl. The band near 890 cm^{-1} was attributed to the semiacetal structure between the aldehyde group and adjacent hydroxyl group. The oxidation degree of OKGM determined by the hydroxylamine hydrochloride method was 43.7%.

Gelation time, morphology, self-healing property and swelling ratio of the OKPP hydrogels

OKPP hydrogels were obtained by the addition of thiol-aldehyde and a Schiff-base reaction. Controlling the gelation time is crucial for designing injectable adhesive hydrogels. First, the gelation time was studied by the influence of the concentration of hydrogel. The gelation time was evaluated by tube inversion. The gelation time decreased as the solid content of polymer in the gel increased (Table 1). This is because the crosslinking rate between functional groups increases with increasing polymer content. In this case, a gelation time that is too long or too short is unfavorable for practical use. We selected a solid content of 15% for the subsequent concentration of hydrogels. Then, we studied the effect of different ratios of γ-PGA-Cys and ε-PL on gelation time. With the increase in the ε-PL ratio, the gelation time was shortened from ~56 ± 6 to ~24 ± 3 s (Table 2). The reason is that ε-PL has a smaller molecular weight than that of γ-PGA-Cys and can increase the chain entanglement between OKGM and ε-PL molecules in the solution, which increases the crosslinking rate between the functional groups. As shown, the OKPP hydrogel precursor can easily form a stable hydrogel (Fig. 3e).

We studied the self-healing ability of OKPP hydrogels. Two pieces of hydrogel with different colors were connected to form a gel (Fig. 3f). After a 60 minutes, the crack disappeared, forming a stable hydrogel. With increasing incubation time, the boundaries between the two different colored hydrogels become blurred. These results indicate the dynamic network and self-healing ability of hydrogels. Thiol-aldehyde addition and Schiff-base reactions are reversible dynamic reactions that are considered to be quasi-covalent. Therefore, hydrogels can automatically repair themselves after rupture. The self-repair function can reduce the risk of wound infection due to accidental rupture of hydrogels.

The OKPP1 hydrogel has the highest swelling rate because the crosslinking rate of the OKPP hydrogel is the lowest (Fig. 3g). The molecular weight of ε-PL is less than that of γ- PGA-Cys, which can increase the chain entanglement between OKGM and ε-PL molecules in solution. With the increase in the ε-PL molar ratio, the crosslinking rate of OKPP increases. The network structure of hydrogels was enhanced by increasing the crosslinking rate. This leads to the water absorption loss.

The multiporous framework of the OKPP hydrogels was investigated by SEM (Fig. 4). The pore sizes of OKPP1, OKPP2, OKPP3, and OKPP4 were between 90 and 150 μm. With the increase in the ε-PL molar ratio, the crosslinking rate of OKPP increases, and the pore size decreases. All OKPP hydrogels were observed to have porous inner structures. The large pore size of the OKPP hydrogel helps cells exchange nutrients, reproduce and migrate.

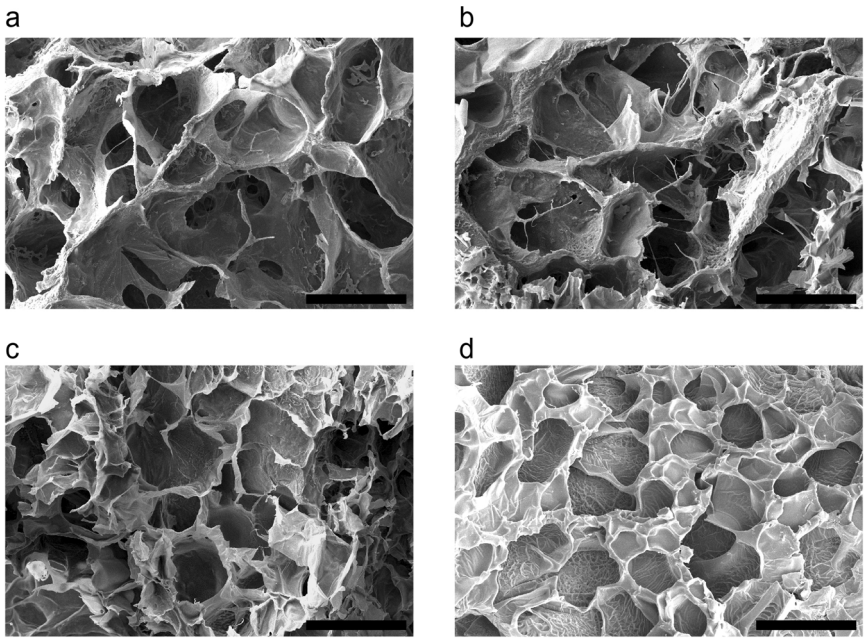

Fig. 4 Morphologies of the OKPP hydrogels. **a** OKPP1. **b** OKPP2. **c** OKPP3. **d** OKPP4. The scale bar is 150 μm.

Determination of the dynamic network of the OKPP hydrogels

We obtained the strain amplitude scanning curve of the OKPP hydrogels and determined the linear viscoelastic domain of the OKPP hydrogels. The results showed that all OKPP hydrogels had stable G′ and G″ in the linear viscoelastic region, indicating that a stable hydrogel structure was formed (Fig. 5a). In addition, we also detected the critical point of hydrogel destruction. With increasing strain, the G′ value sharply dropped to below G″, indicating that the OKPP hydrogel network was destroyed. According to the critical point of the hydrogel strain, the continuous ladder strain method was used to measure the recovery behavior of OKPP hydrogels (Fig. 5b). When the OKPP hydrogels exert 300% strain, the value of G′ decreases rapidly. However, when the hydrogel exerts 0.1% strain, the G′ value can be returned to the original value. The fracture and recovery behaviors of hydrogels were checked several times, indicating that all OKPP hydrogels showed rapid and efficient self-healing ability. Continuous flow experiments show that the OKPP hydrogels exhibit shear thinning behavior under continuous flow conditions, which can be explained by the general reduction in viscosity with increasing shear rate (Fig. 5c). It was proven that the OKPP hydrogel is injectable. As shown, the OKPP hydrogel precursor can be easily injected into the dual channel syringe to form a stable hydrogel (Fig. 5d). In addition, the OKPP hydrogel is transparent at the beginning and becomes darker after exposure to air for 12 h (Fig. S1). This is because L-cysteine in the hydrogel has antioxidant properties, which can slow the oxidation of dopamine.

In vitro antibacterial properties of the OKPP hydrogels

Bacterial infection is a main factor that hinders the healing of burn wounds. Serious infection has a negative impact on the rehabilitation of patients. Antibacterial effects are very important for the development of biological dressings[1,7]. Therefore, two common burn-infected bacteria were used to evaluate the antibacterial activity of OKPP hydrogels (Fig. 6a, b). Compared with the control group, the OKPP hydrogel with added ε-PL exhibits antibacterial activity (OKPP2, OKPP3 and OKPP4). This is because the added ε-PL is a natural antibacterial polypeptide. With the increase in the ε-PL molar ratio, the antibacterial activity of the OKPP hydrogels also increased. The results showed that the OKPP3 and OKPP4 hydrogels could reduce the bacterial level by 10^3 times, and ≥99% of *S. aureus* and *Pseudomonas aeruginosa* were killed. These results showed that the OKPP hydrogels showed high levels of antibacterial activity.

In addition, the morphology of *S. aureus* and *Pseudomonas aeruginosa* after OKPP hydrogel treatment was observed by scanning electron microscopy (SEM). *S. aureus* and *Pseudomonas aeruginosa* were seeded onto the OKPP1 hydrogel as control groups. In the control group, *S. aureus* and *Pseudomonas aeruginosa* all had complete and smooth cell membranes. In contrast, the shape of bacteria in the OKPP3 hydrogel group was both shrunken and deformed (Fig. 6c). This indicates that the

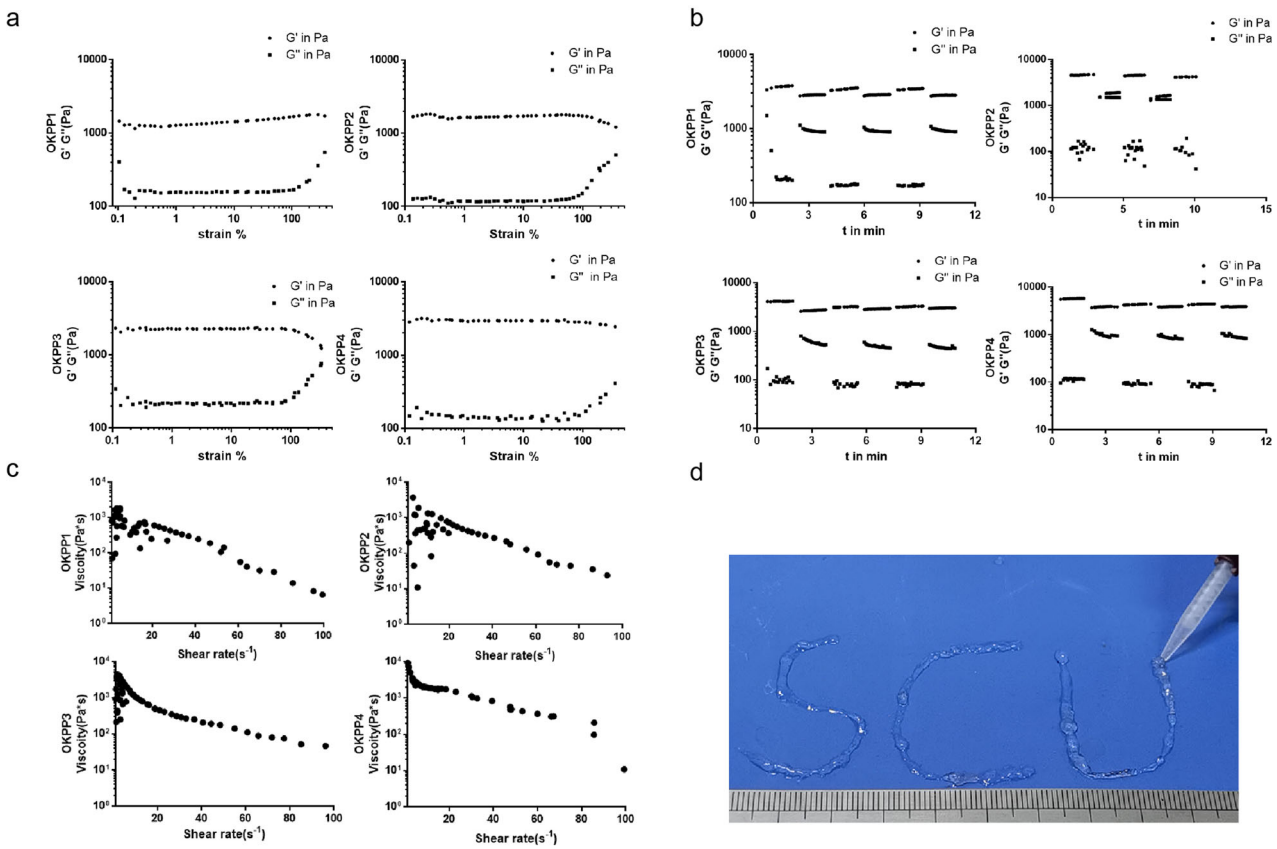

Fig. 5 Rheological characterizations of OKPP hydrogels. a Strain amplitude sweep test. **b** Alternate step strain sweep test. **c** Shear thinning behavior of OKPP hydrogels. **d** Evaluation of the injectability of OKPP hydrogels with an injector.

bacteria were damaged. These results suggest that OKPP hydrogels have antibacterial activity by destroying the cell membrane of *S. aureus* and *Pseudomonas aeruginosa*. Its mechanism of action is similar to that of antimicrobial peptides on microorganisms.

Antioxidant efficiency of the OKPP hydrogels

In infections, excessive production of ROS can lead to cell damage. ROS aggravate the coexpression of inflammatory mediators, leading to the stimulation of tissue necrosis[19,50]. Therefore, increasing antioxidant activity in wound dressings has a positive effect on the process of wound healing. The modified L-cysteine in OKPP hydrogels is a component of glutathione, an important antioxidant in the body. The molecule contains active sulfhydryl (-SH), which can eliminate free radicals in the human body[36,37]. We monitored the ability of OKPP hydrogels to scavenge DPPH free radicals by monitoring the intensity of the DPPH free radical absorption peak at 516 nm (Fig. 7c). All OKPP hydrogels containing γ-PGA-DA-Cys showed an obvious decrease in the intensity of DPPH (Fig. 7a, b). This is due to electron transfer or hydrogen atoms supplied from L-cysteine to DPPH radicals. All OKKP hydrogels have antioxidant activity from γ-PGA-DA-Cys, which can reduce the overdose of ROS.

Adhesive strength tests

Compared with the traditional suture and stapler, the adhesive wound dressing can close the wound by bonding the tissue around the wound, which has advantages in reducing pain and scarring. The dressing can also reduce the risk of wound infection and delayed healing[40]. The thiols of γ-PGA-DA-Cys in hydrogels can react with cysteine residues in tissues to form two sulfur bonds, and dopamine of γ-PGA-DA-Cys can provide hydrogen bonds, thereby enhancing the bonding strength of hydrogels and tissues.

Pig tissue was used as a substrate for the lap shear bond strength test. The bonding strengths of OKPP1, OKPP2, OKPP3, and OKPP4 are approximately 20.9 kPa, 19.2 kPa, 18.3 kPa, and 15.2 kPa, respectively (Fig. 8a, b). The mole ratio of γ-PGA-DA-Cys in the hydrogel increased, and the bond strength of the hydrogel increased. In addition, due to better adhesion, we used OKPP hydrogels (OKPP3 hydrogel as an example) to adhere to two pig skins, and the gels could lift two 100 g weights (Fig. 8c). These

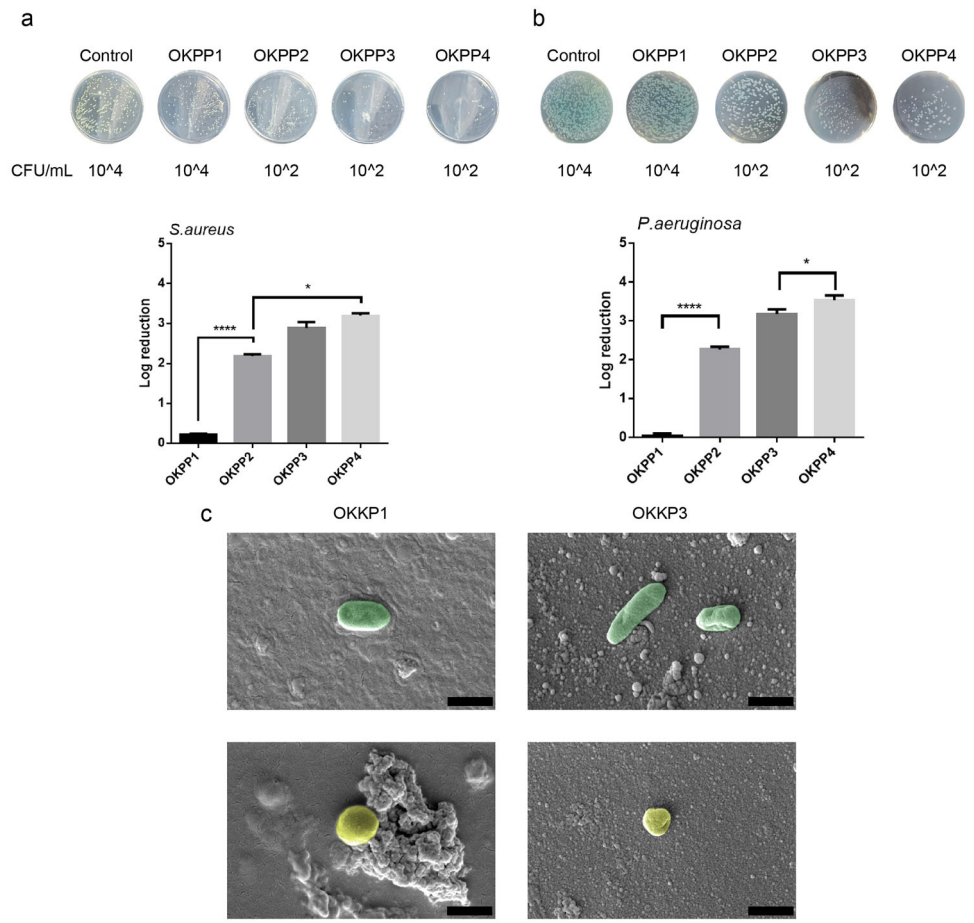

Fig. 6 Evaluation of the antibacterial properties of the hydrogels. a, **b** Evaluation of the resistance of OKPP hydrogels to *S. aureus* and *Pseudomonas aeruginosa*. The colony count on different groups of LB plate was the result after dilution. **c** SEM images of *S. aureus* and *Pseudomonas aeruginosa* seeded on the OKPP hydrogel. The scale bar is 1 μm. $^{*}P < 0.05$, $^{****}P < 0.0001$.

results indicate that the OKPP hydrogel has good adhesion strength and can adhere to the skin surface as a wound dressing.

Cytocompatibility evaluation of the hydrogel

As a wound dressing for wound healing, the biocompatibility of OKPP hydrogels is also important. Due to the high antibacterial activity, good antioxidant activity and adhesive strength of the OKPP3 hydrogel, we measured its cytotoxicity. NIH 3T3 cells were used to evaluate the cytotoxicity of OKPP3 hydrogel extracts. After incubation for 24, 48 and 72 h in the presence of 15, 1.5, 0.5, and 0.15 mg/mL extracts. Compared with the control groups, the hydrogels showed no obvious cytotoxicity, with over 90% of the cells remaining viable (Fig. 9a). The results of live/dead fluorescence staining showed that compared with the control group, the spindle shape and proliferation of NIH 3T3 cells in the OKPP3 group were normal (Fig. 9b). This indicates that the OKPP3 hydrogel exibits no obvious cytotoxicity.

In vitro ROS scavenging effect of the OKPP hydrogel

When the wound is infected and produces oxidative stress, the absorption of oxygen (O_2) by phagocytes increases. Then, a considerable amount of ROS is produced by the conversion of O_2 to superoxide followed by the conversion of superoxide into hydrogen peroxide[19,50,51]. Excessive H_2O_2 can cause oxidative damage to cells. We used NIH 3T3 cells to evaluate the ROS scavenging capacity of the OKPP3 hydrogel in vitro (Fig. 10). Compared with the H_2O_2 treatment group, the survival rate of NIH 3T3 cells was improved after pretreatment with the OKPP3 hydrogel. It was proven that the OKPP hydrogel effectively protected H_2O_2.

Wound closure

We used the OKPP3 hydrogel and 3 M Tegaderm^{TM} commercial dressing to treat mouse full-thickness burn infection models. As shown in Fig. 11a, the OKPP hydrogel was used to cover the wound in the OKPP3 group, and the wound was exposed in the untreated

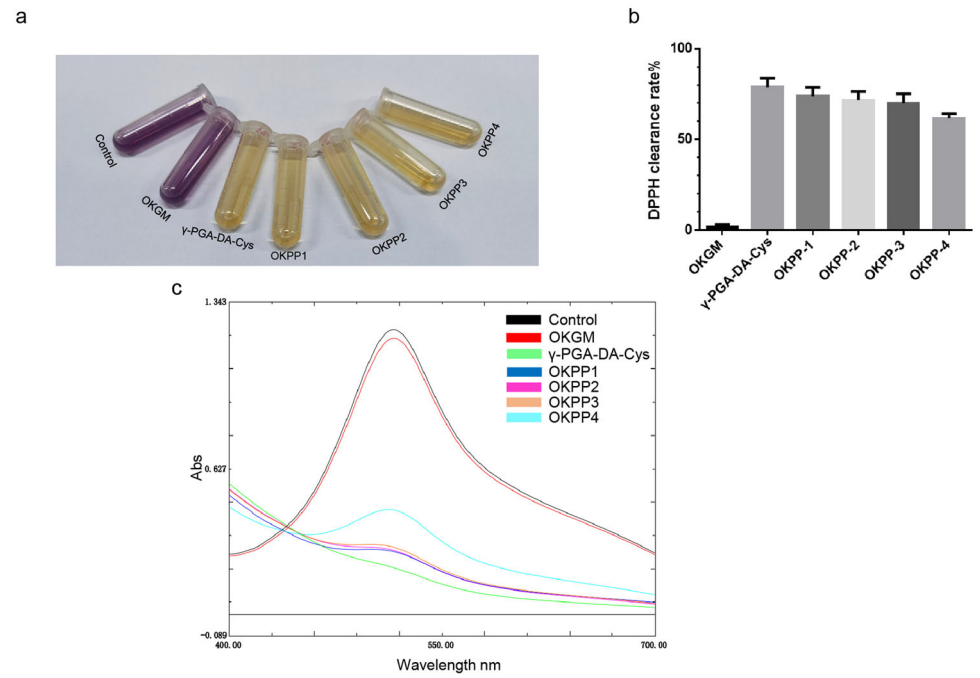

Fig. 7 Antioxidant efficiency of OKPP hydrogels. a Color changes of different groups after incubation with DPPH for 30 min. **b** DPPH scavenging effect of different groups. **c** UV–vis spectra of different groups after incubation with DPPH for 30 min.

group. On day 3, the wound in the OKPP3 group was still covered by the OKPP hydrogel, and the wound was more contracted than that in the other two groups. Compared with the untreated group, the Tegaderm™ film group had no obvious suppuration. In addition, the untreated group contained edema and suppurative infection. On day 7, the wound surface of the OKPP3 group was still covered by some OKKP hydrogel, and the degree of wound healing was larger than that of the other two groups. The degree of wound healing in the Tegaderm™ film group was greater than that of the untreated group. The wounds in the untreated group began to scab and healed. On day 14, more than half of the wounds healed in the OKPP3 group. The wounds of each group began to shrink and darken. The scab on the surface of each group contracted. On day 21, the OKPP3 group showed the best healing effect and was almost completely healed (Fig. 11b). Following the Tegaderm™ film group, a small number of wounds remained that did not heal. The untreated group also contained some exposed wounds.

The antibacterial effect was evaluated by calculating the number of bacteria in the skin tissue homogenate of different groups on day 14. Compared with the control group and Tegaderm™ film group, the OKPP group had the lowest bacterial burden and showed a good antibacterial effect (Fig. 11c). It was proven that the OKPP hydrogel has certain antibacterial properties in vivo.

The wound tissue was stained with H&E and Masson's trichrome on days 7, 14, and 21 (Fig. 12). Various tissue structures, such as inflammation, fibroblasts, capillaries and epithelial cell proliferation, were observed under an optical microscope. On day 7, the number of inflammatory cells decreased in the OKPP3 group and commercial dressing group. The commercial dressing group and the untreated group had thicker scabs, while the untreated group contained more inflammation. On day 14, some new epithelial tissues were observed in the OKPP group and commercial dressing group, and the inflammation was also reduced. The untreated group still contained thick scabs, and the inflammation was also reduced compared with that on day 7. On day 21, the wounds treated in the OKPP group were covered by epithelial tissue, and new hair follicles were produced. In addition, more collagen tissue was observed in the OKPP group (Fig. S2). These results indicate that the OKPP hydrogel can help epithelial tissue form. The OKPP hydrogel exhibits a therapeutic effect on wound healing.

Immunohistochemical staining

TGF-β is involved in processes of wound healing, such as fibroblast proliferation and collagen synthesis. TGF-β also plays a crucial role in promoting further inflammation[27,51]. On day 7, all groups exhibited strong TGF-β expression (Fig. 13a). On day 14, TGF-β expression

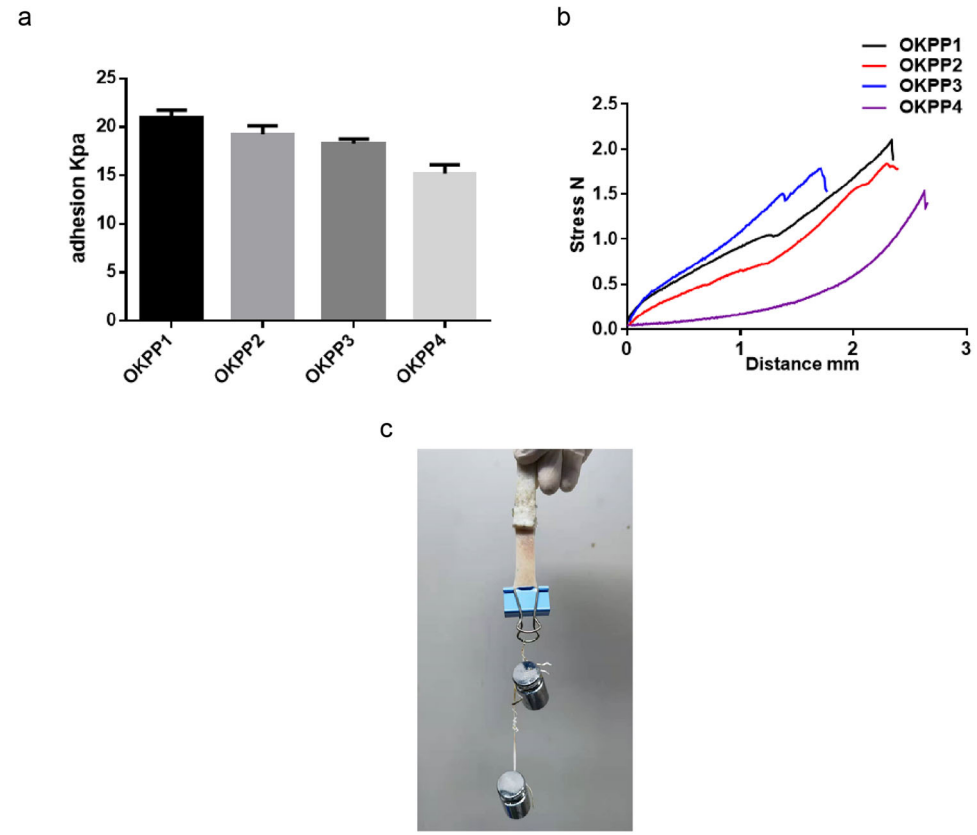

Fig. 8 Adhesive strength tests of OKPP hydrogels. a Adhesive strength of OKPP hydrogels. **b** Stress–displacement curves. **c** Photo of pig skin bonded by the OKPP hydrogel. The weight suspended under the pig skin was 100 × *g*.

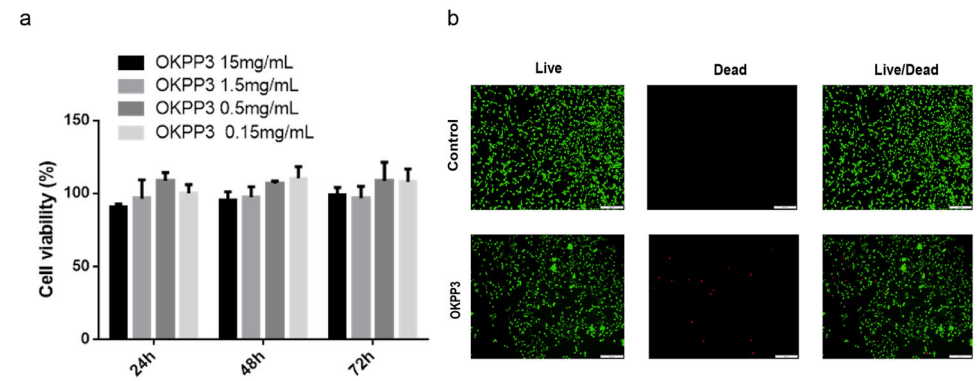

Fig. 9 In vitro cytotoxicity evaluation of OKPP hydrogels. a Cell viability. **b** Live/dead staining. The scale bar is 200 μm.

decreased in all groups. This shows that in the whole repair process, the expression of TGF-β showed a general trend of decreasing with time. In addition, the expression of TGF-β in the OKPP3 group was lower than that in the Tegaderm™ film group and the control group. This shows that the OKPP3 group can effectively control inflammation and plays a positive role in the whole repair process. CD31 is used to evaluate angiogenesis in wound repair[27,40]. Compared with the control group and commercial dressing group, higher CD31 expression and more angiogenesis were observed (Fig. 13b). These results indicate that the OKPP hydrogel can promote wound healing, reduce wound inflammation and promote angiogenesis.

Conclusions

In this study, we designed an injectable hydrogel with antibacterial activity and antioxidant activity. The hydrogel is gelled by the addition of thiol-aldehyde and the Schiff-base reaction. This hydrogel performs quick and controllable gelation and exhibits good self-healing ability. Importantly, the hydrogel has good antibacterial activity against *Staphylococcus aureus* and *Pseudomonas aeruginosa* and has certain antioxidant and adhesion properties. In in vivo full-thickness burn infection models, this hydrogel has the ability to reduce inflammation, exhibits effective antibacterial activity and promotes wound regeneration. These results show that this hydrogel has certain potential in wound dressings. We will further evaluate and optimize the antibacterial, adhesion and antioxidant effects of this hydrogel. We will develop other potential biomedical applications of this hydrogel, such as the transportation of drugs or bioactive substances for local delivery in tissue regeneration.

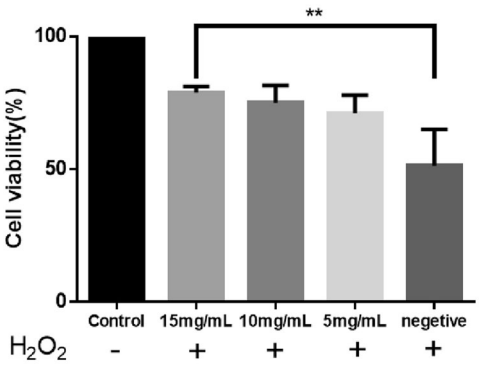

Fig. 10 Cell viability of NIH 3T3 cells under different treatment conditions with H_2O_2. Except the control group, the other groups were treated with 250 μM H_2O_2. The concentration of OKPP3 hydrogel were 15, 10 and 5 mg/mL respectively. $^{**}P < 0.01$.

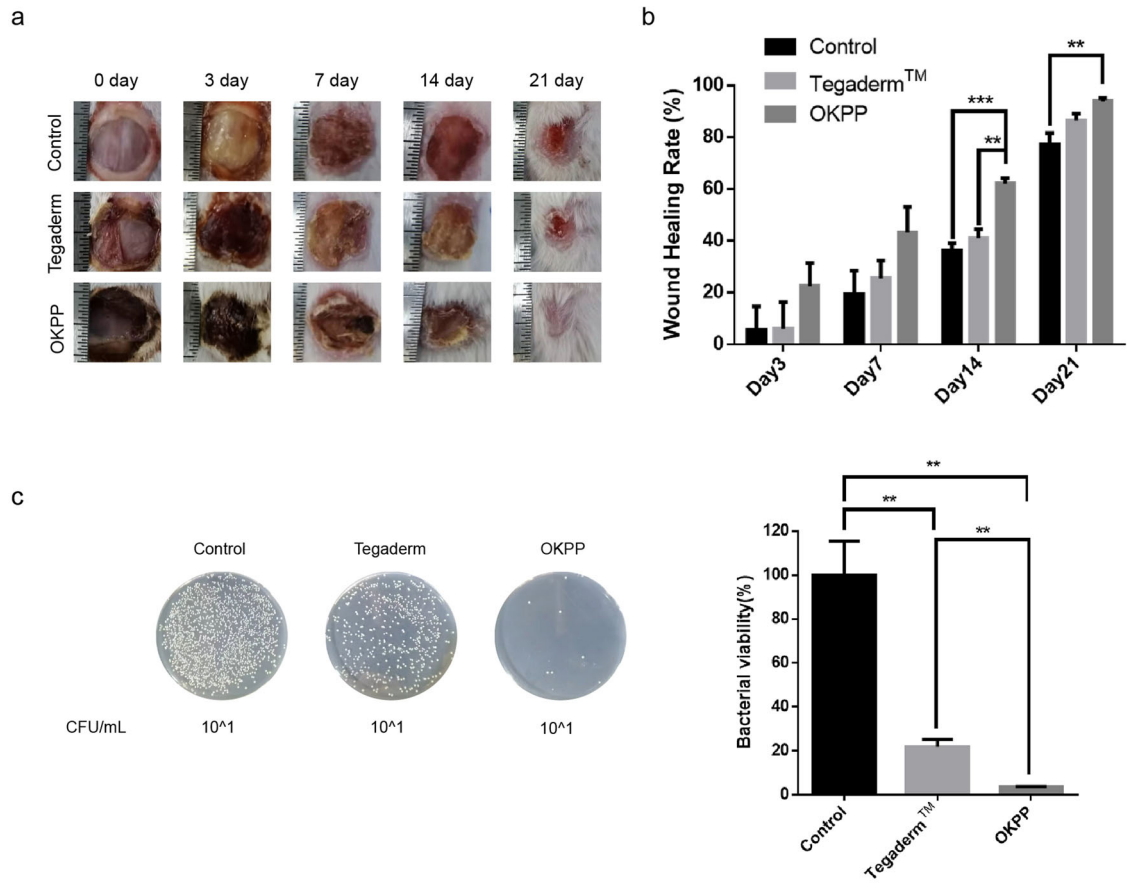

Fig. 11 Evaluation of the OKPP hydrogel in vivo for skin repair and wound healing. a Photo images of wound healing after 3, 7, 14, and 21 days. **b** Wound healing effect analysis. **c** The corresponding agar plate image of the *S. aureus* burden of infected wound tissues. $^{*}P < 0.05$, $^{**}P < 0.01$, $^{***}P < 0.001$. The scale of the ruler used is 0.1 cm.

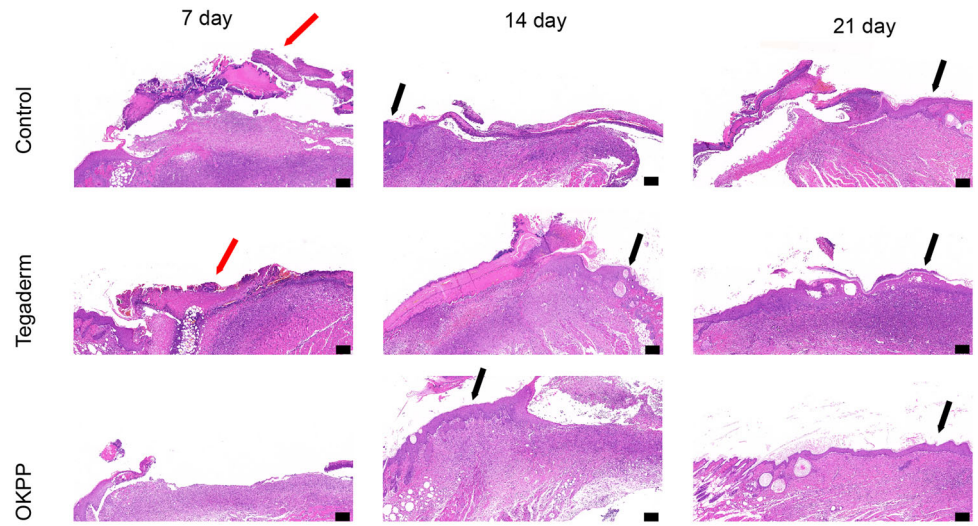

Fig. 12 H&E staining of wound tissue on days 7, 14, and 21. The red arrows show scar tissue. The black arrows show epithelial tissue. The scale bar is 200 μm.

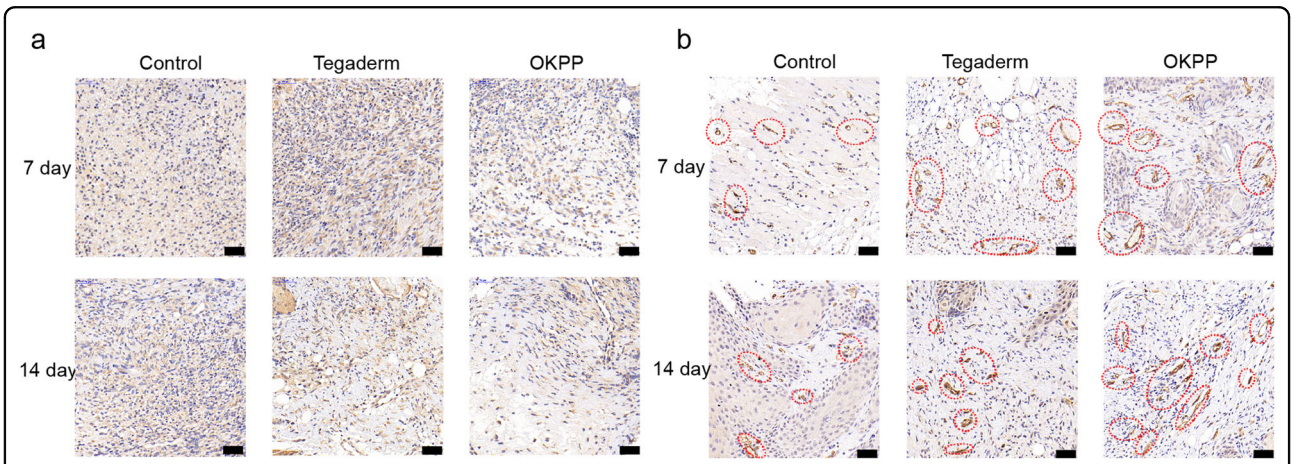

Fig. 13 Immunohistochemical staining analysis. a Immunohistochemical staining analysis of TGF-β. The brown substance in Fig. 13a is TGF-β. **b** Immunohistochemical staining analysis of CD31. The red circle shows CD31. The scale bar is 200 μm.

Acknowledgements
Z.Q. and X.W. supervised this study and provided intellectual guidance. A.S. and X.H. designed and synthesized the hydrogels. D.H. contributed to the in vitro experiments. T.L. contributed to the in vivo animal experiment. X.J. collated and analyzed the experimental data. The main experiments and the writing of the manuscript were completed by A.S. This work was financially supported by the National Natural Science Fund for Distinguished Young Scholars (NSFC31525009), the National Natural Science Foundation of China (NSFC31930067, 31771096), the National Key Research and Development Program of China (No. 2017YFC1103502) and the 1·3·5 project for disciplines of excellence, West China Hospital, Sichuan University (ZYGD18002).

Author details
[1]State Key Laboratory of Biotherapy/Collaborative Innovation Center for Biotherapy, West China Hospital, West China Medical School, Sichuan University, 610041 Chengdu, P.R. China. [2]Department of Cardiovascular Surgery, West China Hospital, Sichuan University, 610041 Chengdu, P.R. China. [3]Laboratory of Aging Research and Cancer Drug Target, State Key Laboratory of Biotherapy, National Clinical Research Center for Geriatrics, West China Hospital, Sichuan University, 610041 Chengdu, P.R. China

Competing interests
The authors declare no competing interests.

Supplementary information The online version contains supplementary material available at https://doi.org/10.1038/s41427-022-00434-z.

Received: 25 May 2022 Revised: 2 September 2022 Accepted: 9 September 2022.
Published online: 4 November 2022

References

1. Markiewicz-G. A. et al. Burn wound healing: clinical complications, medical care, treatment, and dressing types: the current state of knowledge for clinical practice. *Int. J. Environ. Res. Public Health*. **19**, 1338 (2022).
2. Greenhalgh, D. G. Management of burns. *N. Engl. J. Med.* **380**, 2349–2359 (2019).
3. Pereira, R. F., Barrias, C. C., Granja, P. L. & Bartolo, P. J. Advanced biofabrication strategies for skin regeneration and repair. *Nanomedicine* **8**, 603–621 (2013).
4. Rowan, M. P. et al. Burn wound healing and treatment: review and advancements. *Crit. Care* **19**, 243 (2015).
5. Stanojcic, M., Vinaik, R. & Jeschke, M. G. Status and challenges of predicting and diagnosing sepsis in burn patients. *Surg. Infect.* **19**, 168–175 (2018).
6. MacNeil, S. Progress and opportunities for tissue-engineered skin. *Nature* **445**, 874–880 (2007).
7. Wang, Y. W. et al. Burn injury: challenges and advances in burn wound healing, infection, pain and scarring. *Adv. Drug Deliv. Rev.* **123**, 3–17 (2018).
8. Atiyeh, B. S., Gunn, S. W. & Hayek, S. N. State of the art in burn treatment. *World J. Surg.* **29**, 131–148 (2005).
9. Weng, T. T. et al. 3D bioprinting for skin tissue engineering: Current status and perspectives. *J. Tissue Eng.* **12**, 20417314211028574 (2021).
10. Bay, C. et al. Comparison of skin substitutes for acute and chronic wound management. *Semin. Plast. Surg.* **35**, 171–180 (2021).
11. Mofazzal Jahromi, M. A. et al. Nanomedicine and advanced technologies for burns: preventing infection and facilitating wound healing. *Adv. Drug Deliv. Rev.* **123**, 33–64 (2018).
12. Groeber, F., Holeiter, M., Hampel, M., Hinderer, S. & Schenke-Layland, K. Skin tissue engineering — in vivo and in vitro applications. *Adv. Drug Deliv. Rev.* **63**, 352–366 (2011).
13. Zhou, W. J. et al. Quantum dots-hydrogel composites for biomedical applications. *Chin. Chem. Lett.* **33**, 1245–1253 (2022).
14. Wang, C. G. et al. Engineering bioactive self-healing antibacterial exosomes hydrogel for promoting chronic diabetic wound healing and complete skin regeneration. *Theranostics* **9**, 65–76 (2019).
15. Pan, P. P. et al. A fast on-demand preparation of injectable self-healing nanocomposite hydrogels for efficient osteoinduction. *Chin. Chem. Lett.* **32**, 2159–2163 (2021).
16. Cheng, L. et al. Injectable polypeptide-protein hydrogels for promoting infected wound healing. *Adv. Funct. Mater.* **30**, 2001196 (2020).
17. Liang, Y., Li, Z., Huang, Y., Yu, R. & Guo, B. Dual-dynamic-bond cross-linked antibacterial adhesive hydrogel sealants with on-demand removability for post-wound-closure and infected wound healing. *ACS Nano* **15**, 7078–7093 (2021).
18. Liu, Y., Yang, Y., Wang, C. & Zhao, X. Stimuli-responsive self-assembling peptides made from antibacterial peptides. *Nanoscale* **5**, 6413–6421 (2013).
19. Rahal, A. et al. Oxidative stress, prooxidants, and antioxidants: the interplay. *Biomed. Res. Int.* **2014**, 761264 (2014).
20. Dong, R., Zhao, X., Guo, B. & Ma, P. X. Self-healing conductive injectable hydrogels with antibacterial activity as cell delivery carrier for cardiac cell therapy. *ACS Appl. Mater. Interfaces* **8**, 17138–17150 (2016).
21. Tian, R. et al. Fabrication of self-healing hydrogels with on-demand antimicrobial activity and sustained biomolecule release for infected skin regeneration. *ACS Appl. Mater. Interfaces* **10**, 17018–17027 (2018).
22. Hong, Y., Gong, Y., Gao, C. & Shen, J. Collagen-coated polylactide microcarriers/chitosan hydrogel composite: Injectable scaffold for cartilage regeneration. *J. Biomed. Mater. Res. Part A* **85A**, 628–637 (2008).
23. Liu, P. et al. Ionic liquid functionalized non-releasing antibacterial hydrogel dressing coupled with electrical stimulation for the promotion of diabetic wound healing. *Chem. Eng. J.* **415**, 129025 (2021).
24. Yu, H. & Xiao, C. Synthesis and properties of novel hydrogels from oxidized konjac glucomannan crosslinked gelatin for in vitro drug delivery. *Carbohydr. Polym.* **72**, 479–489 (2008).
25. Zhu, L., Chen, J., Mao, X. & Tang, S. A γ-PGA/KGM-based injectable hydrogel as immunoactive and antibacterial wound dressing for skin wound repair. *Mater. Sci. Eng. C* **129**, 112374 (2021).
26. Kanniyappan, H., Thangavel, P., Chakraborty, S., Arige, V. & Muthuvijayan, V. Design and evaluation of Konjac glucomannan-based bioactive interpenetrating network (IPN) scaffolds for engineering vascularized bone tissues. *Int. J. Biol. Macromol.* **143**, 30–40 (2020).
27. Liang, Y., Zhao, X., Hu, T., Han, Y. & Guo, B. Mussel-inspired, antibacterial, conductive, antioxidant, injectable composite hydrogel wound dressing to promote the regeneration of infected skin. *J. Colloid Interface Sci.* **556**, 514–528 (2019).
28. Li, S. D. et al. Bioinspired double-dynamic-bond crosslinked bioadhesive enables post-wound closure care. *Adv. Funct. Mater.* **30**, 2000130 (2020).
29. Zhou, C. C. et al. A photopolymerized antimicrobial hydrogel coating derived from epsilon-poly-l-lysine. *Biomaterials* **32**, 2704–2712 (2011).
30. Wang, R. et al. A biomimetic mussel-inspired ε-poly-l-lysine hydrogel with robust tissue-anchor and anti-infection capacity. *Adv. Funct. Mater.* **27**, 1604894 (2017).
31. Xu, H.-L. et al. Thiolated γ-polyglutamic acid as a bioadhesive hydrogel-forming material: evaluation of gelation, bioadhesive properties and sustained release of KGF in the repair of injured corneas. *Biomater. Sci.* **7**, 2582–2599 (2019).
32. Buescher, J. M. & Margaritis, A. Microbial biosynthesis of polyglutamic acid biopolymer and applications in the biopharmaceutical, biomedical and food industries. *Crit. Rev. Biotechnol.* **27**, 1–19 (2007).
33. Tong, Z. R. et al. In situ synthesis of poly (γ- glutamic acid)/alginate/AgNP composite microspheres with antibacterial and hemostatic properties. *Carbohydr. Polym.* **221**, 21–28 (2019).
34. Yang, R. et al. Bioinspired poly (γ-glutamic acid) hydrogels for enhanced chondrogenesis of bone marrow-derived mesenchymal stem cells. *Int. J. Biol. Macromol.* **142**, 332–344 (2020).
35. Weng, Y., Cao, Y., Arevalo, C., Vacanti, M. P. & Vacanti, C. A. Tissue-engineered composites of bone and cartilage for mandible condylar reconstruction. *J. Oral. Maxillofac. Surg.* **59**, 185–190 (2001).
36. Mirończuk-Chodakowska, I., Witkowska, A. M. & Zujko, M. E. Endogenous non-enzymatic antioxidants in the human body. *Adv. Med. Sci.* **63**, 68–78 (2018).
37. Ulrich, K. & Jakob, U. The role of thiols in antioxidant systems. *Free Radic. Biol. Med.* **140**, 14–27 (2019).
38. Bernkop-Schnürch, A., Schwarz, V. & Steininger, S. Polymers with thiol groups: a new generation of mucoadhesive polymers? *Pharm. Res.* **16**, 876–881 (1999).
39. Wang, L., Li, Y., Lin, L., Mu, R. & Pang, J. Novel synthesis of mussel inspired and Fe3+ induced pH-sensitive hydrogels: Adhesion, injectable, shapeable, temperature properties, release behavior and rheological characterization. *Carbohydr. Polym.* **236**, 116045 (2020).
40. He, X. Y. et al. Mussel-inspired antimicrobial gelatin/chitosan tissue adhesive rapidly activated in situ by H^2O^2/ascorbic acid for infected wound closure. *Carbohydr. Polym.* **247**, 116692 (2020).
41. Han, L. et al. Mussel-inspired adhesive and tough hydrogel based on nanoclay confined dopamine polymerization. *ACS Nano* **11**, 2561–2574 (2017).
42. Liao, M. H. et al. Wearable, healable, and adhesive epidermal sensors assembled from mussel-inspired conductive hybrid hydrogel framework. *Adv. Funct. Mater.* **27**, 1703852 (2017).
43. Fan, C., Fu, J., Zhu, W. & Wang, D.-A. A mussel-inspired double-crosslinked tissue adhesive intended for internal medical use. *Acta Biomater.* **33**, 51–63 (2016).
44. Chen, H. L. et al. An injectable self-healing hydrogel with adhesive and antibacterial properties effectively promotes wound healing. *Carbohydr. Polym.* **201**, 522–531 (2018).
45. Yang, R. et al. Injectable adaptive self-healing hyaluronic acid/poly (γ-glutamic acid) hydrogel for cutaneous wound healing. *Acta Biomater.* **127**, 102–115 (2021).
46. Gharibi, R., Yeganeh, H., Rezapour-Lactoee, A. & Hassan, Z. M. Stimulation of wound healing by electroactive, antibacterial, and antioxidant polyurethane/siloxane dressing membranes: in vitro and in vivo evaluations. *ACS Appl. Mater. Interfaces* **7**, 24296–24311 (2015).
47. Zhang, D.-Y. et al. Multi-enzyme mimetic ultrasmall iridium nanozymes as reactive oxygen/nitrogen species scavengers for acute kidney injury management. *Biomaterials* **271**, 120706 (2021).
48. Zhu, Q. Y. et al. Enhanced healing activity of burn wound infection by a dextran-HA hydrogel enriched with sanguinarine. *Biomater. Sci.* **6**, 2472–2486 (2018).
49. Huang, H. et al. Injectable hydrogel for postoperative synergistic photothermal-chemodynamic tumor and anti-infection therapy. *Biomaterials* **280**, 121289 (2022).
50. Church, D., Elsayed, S., Reid, O., Winston, B. & Lindsay, R. Burn wound infections. *Clin. Microbiol. Rev.* **19**, 403–434 (2006).
51. Zheng, Y. Y. et al. Injectable supramolecular gelatin hydrogel loading of resveratrol and histatin-1 for burn wound therapy. *Biomater. Sci.* **8**, 4810–4820 (2020).